Electronic Journal of Structural Engineering

Original Article

Cite this: DOI:10.56748/ejse.26947

Received Date: 12 December 2025
Accepted Date: 19 May 2026

1443-9255
https://ejsei.com/ejse

Exploring the Connection Between Ultimate Punching Resistance and Failure Mode of Slab-Column Joints with Machine Learning Algorithms

Huajun Yan [a*], Zuohua Li [a], Chao Gong [b], Dandan Shen [c]

[a] School of Intelligent Civil and Ocean Engineering, Harbin Institute of Technology Shenzhen, Shenzhen 518055, China;
[b] Central Research Institute of Building and Construction (Shenzhen) Co., Ltd., MCC Group, Shenzhen 518055, China;
[c] SANY Heavy Industry Co., LTD, Beijing 100044, China;
* Corresponding author: 19115044@bjtu.edu.cn

Abstract

While reinforced concrete (RC) flat slab systems offer advantages in terms of architectural flexibility and construction efficiency, they remain susceptible to abrupt punching shear failures at slab-column joints. The current methods for assessing failure modes and punching resistance exhibit considerable limitations, primarily owing to an incomplete understanding of the relationship between failure progression and ultimate resistance, which introduces substantial uncertainty into predictive estimations. This study addresses the persistent challenge of determining a quantitative correlation between failure mode evolution and punching shear capacity through the application of machine learning (ML) algorithms. A methodology for identifying failure modes is presented using three ML algorithms (DT, RF, and XGBoost) along with an approach for accurately predicting punching resistance. This approach integrates the actual failure modes as fundamental input features and further enhances predictive performance through two metaheuristic optimization (BFO and GWO) techniques. The BFO-XGBoost model exhibited superior performance in both failure mode classification (F1=93.8%, Acc=98.3%) and punching resistance prediction (R2 = 0.967, MAE = 0.032MN, and RMSE = 0.049MN). Shapley additive explanations (SHAP) analysis was employed to assess model interpretability, enabling the identification of critical parameters and their interactions. It offers unique insights into the mechanism by which failure characteristics are related to ultimate resistance, as well as practical recommendations for mitigating brittle failure risks and enhancing ultimate resistance.

Keywords

Slab-column joint, Punching resistance, Failure mode, Metaheuristic optimization, Machine learning, Shapley additive explanations

1. Introduction

In commercial infrastructure, including shopping complexes and parking facilities, reinforced concrete (RC) slab-column structures are commonly utilized, as they employ interconnected slabs and columns without beams, thereby optimizing the utilization of available space (Yan and Xie, 2024). A slab column joint is one of the most critical nodes in such structures, since they suffer from axial loads and unbalanced bending moments, and are susceptible to flexural failures and punching shear failures. As shown in Fig. 1, an unexpected punching shear breakout emerged from the slab without prior indications, possibly resulting in a progressive collapse of the entire structure (Makoond et al., 2024). A notable structural failure such as the Champlain Towers South disaster in recent years has catalyzed intensive research into this potentially dangerous failure mode (Shen et al., 2022).

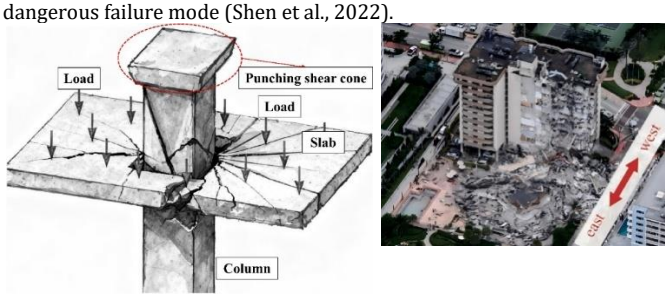

(a) (b)

Fig. 1 Punching shear failure of slab-column joints: (a) Punching shear failure mechanism schematic; (b) Exemplification of localized damage initiation leading to cascading progressive collapse (Makood et al., 2024).

With rigorous investigations into its key governing parameters, significant advances have been made in predicting the punching shear resistance of slabs (Al-Mhawish et al., 2025; Monserrat-López et al., 2025; Hanoon et al., 2025; Ewees MH et al., 2024). However, it remains relatively rare to find theoretical studies about the prediction of failure modes for slabs (Liang et al., 2022). The lack of quantitative correlations between critical parameters and failure mechanisms in slab-column joints results in considerable ambiguity when assessing punching shear capacity.

In previous research by Gesund and Kaushik (1970), yield line theory was employed to categorize failure mechanisms in slabs under punching shear, which provides an empirical model for interpreting structural behavior of slab-column joints. Randame (1996) developed a formula for categorizing failure modes following previous research efforts, highlighting the importance of the shear span ratio. Leveraging these developments, Xiao and Chin (2007) established a novel failure mechanism classification criterion for punching shear in slabs. In spite of this, inherent simplifications adopted during the theoretical development of these empirical models led to the exclusion of key influencing factors from final predictive equations. Furthermore, the initial scarcity of validation data for these models implies that their empirical parameters remain subject to further calibration.

Data-driven models have been significantly accelerated by recent breakthroughs in artificial intelligence (AI) technologies (Kumarawadu et al., 2024; Yang et al., 2025; Ren et al., 2025; Wang, 2025). The widespread and successful deployment of machine learning (ML) across a multitude of fields has established it as the preeminent field of scientific inquiry. A range of ML models, including Artificial Neural Networks (ANN), Light Gradient-Boosting (LGBT), Adaptive Boosting (AdaBoost), Extreme Gradient Boosting (XGBoost) and Category Boosting (CatBoost) algorithms have been utilized to predict the punching shear resistance (Abbas and Alsaif, 2025; Babiker et al., 2025; Elaal et al., 2025; Khajavi et al., 2025; Zheng et al., 2025). Compared to established design code provisions, ML models significantly enhance prediction accuracy.

There has been recent research showing the potential of ML methods to identify failure modes in slab-column joints. Specifically, Liang et al. (2022) and Shen et al. (2022) employed seven distinct ensemble learning methods to investigate the failure behavior of slabs. According to empirical validation, the proposed data-driven methods significantly improve the accuracy of failure mode prediction. Nevertheless, the depth of discussion in these works remains limited. For instance, failure modes and ultimate resistance are treated separately as analytical points, without any exploration of their interdependencies or the concurrent influence of multiple variables on both responses. A fragmented approach hinders a comprehensive understanding of how failure modes relate to ultimate

resistance. Furthermore, the lack of algorithm optimization for parameter tuning is noteworthy, as existing evidence suggests that models that are not optimized rigorously are likely to perform poorly (Wu and Zhou, 2023).

The objective of this study is to develop an optimized ML framework that can predict both the mode of failure and the ultimate resistance of slab-column joints. A key novelty of this study is to treat failure mode as one of the input variables, thereby improving prediction accuracy and allowing investigation of the inherent relationship between failure mode and ultimate resistance. Finally, a new method is introduced that simultaneously enhances the punching shear resistance of slab-column joints while reducing undesirable failure modes.

2. Deployment of machine learning approaches

2.1 Ensemble Learning Models

Three ensemble learning models are employed in this study, namely decision trees (DT), random forests (RF), and extreme gradient boosting (XGBoost), to predict failure modes and estimate the punching shear resistance.

In DT, the continuous predictor space is split iteratively according to a set of optimization criteria, resulting in leaf nodes that provide specific predictions of the target value. In contrast to leaf nodes, which are characterized by the absence of outgoing edges, root and internal nodes are commonly classified as root or internal nodes (Tusher et al., 2025). In order to enhance prediction performance, the RF algorithm incorporates multiple decision trees through an ensemble approach. By generating an ensemble of decision trees and averaging their predictions, RF algorithms are able to effectively address the challenges associated with high variance and overfitting (Parisi et al., 2025). In contrast to bagging, XGBoost is an advanced boosting algorithm that exhibits significant correlation and dependency among its base learners (Ren and Liu, 2025). The XGBoost algorithm provides three primary enhancements within the gradient boosting: model performance and complexity are maintained by incorporating a structural risk term in the objective function; adoption of a structural gain metric as the branching criterion for generating more straightforward overall structures; a structural gain metric may be adopted as the branching criterion for generating more straightforward overall structures (Tusher et al., 2025; Parisi et al., 2025; Ren and Liu, 2025).

2.2 Strategies for hyperparameter configuration

Conventional approaches to hyperparameter tuning in ensemble models, such as the XGBoost model, have certain limitations: (1) grid search is hindered by dimensionality in the XGBoost hyperparameter space due to its high dimensions; (2) random searches lack targeted exploration and often find suboptimal areas on complex non-convex terrain; (3) Bayesian optimization relies on surrogate models (such as Gaussian processes), though dealing with classification and discrete hyperparameters can be challenging. Consequently, this study employs grey wolf optimization (GWO) and bacterial foraging optimization (BFO) to tune the target parameters, and the efficacy of these two optimization techniques has been validated in previous investigations (Alizamir et al., 2025; Laouissi et al., 2025; Alkhonaini et al., 2025).

The grey wolf optimization (GWO) algorithm simulates the social hierarchy of grey wolves by assigning the three best-fit solutions as α, β, and δ wolves, while designating the remaining candidate solutions as ω wolves. Two major behavioral principles are followed in simulations: hierarchical dominance and cooperative predation. It can be seen in Fig. 2 that both social hierarchy and dynamic updating of target positions are incorporated into the collective hunting behavior of grey wolves. The following formula is used in the updating process.

$$\vec{D} = \left|\vec{C} \cdot \vec{X}_{Target}(t) - \vec{X}(t)\right| \quad (1)$$

$$\vec{X}(t+1) = \vec{X}_{Target}(t) - \vec{A} \cdot \vec{D} \quad (2)$$

Where $\vec{X}$ represents the current position of wolves; $\vec{X}_{Target}$ represents the target position; $\vec{A}$ and $\vec{D}$ denote the coefficient vectors.

For the equation to meet the optimality condition, it must be formulated as follows:

$$\begin{cases} \vec{D}_\alpha = \left|\vec{C}_1 \cdot \vec{X}_\alpha(t) - \vec{X}(t)\right| \\ \vec{D}_\beta = \left|\vec{C}_2 \cdot \vec{X}_\beta(t) - \vec{X}(t)\right| \\ \vec{D}_\delta = \left|\vec{C}_3 \cdot \vec{X}_\delta(t) - \vec{X}(t)\right| \end{cases} \quad (3)$$

$$\vec{X}(t+1) = \left(\vec{X}_1 + \vec{X}_2 + \vec{X}_3\right) \quad (4)$$

Positional vectors are dynamically adjusted by the search agent to achieve asymptotically convergence. After identifying the global optimum, a solution convergence is achieved by satisfying the iterative termination criteria.

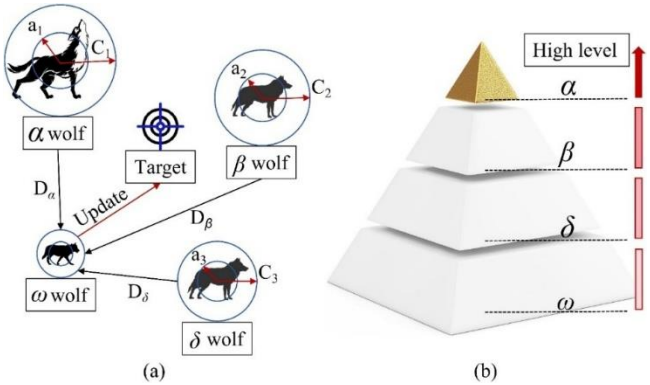

Fig. 2 GWO algorithm: (a) Dynamic updating of target positions; (b) Social hierarchy

In the bacterial foraging optimization (BFO), Escherichia coli foraging strategies are abstracted and computationally formalized (Fig. 3). As version of this algorithm mimics the process by which bacteria sense and navigate chemical gradients in their environment so that they can move toward nutrient-rich areas, and it has four core behavior components:

Chemotaxis: The concept of chemotaxis is based on two alternating actions, tumbling, which involves a change in direction at random, and swimming, which involves sustained motion in a favorable direction, with the following calculation formulas being relevant:

$$\vec{\theta}_n(i+1,j,k) = \vec{\theta}_n(i,j,k) + \vec{D}_n \cdot d_{ctn} \quad (5)$$

$$d_{ctn} = \frac{\Delta(n)}{\sqrt{\Delta^T(n)\Delta(n)}} \quad (6)$$

Where the indices i, j, k denote the number of bacterial individuals for chemotaxis, reproduction, and elimination-dispersal operation; $\vec{\theta}_n$ represents the position state of the n-th bacterium; $\vec{D}_n$ measures the maximum displacement during chemotaxis; Δ indicates a direction vector with components constrained to a range of [-1, 1].

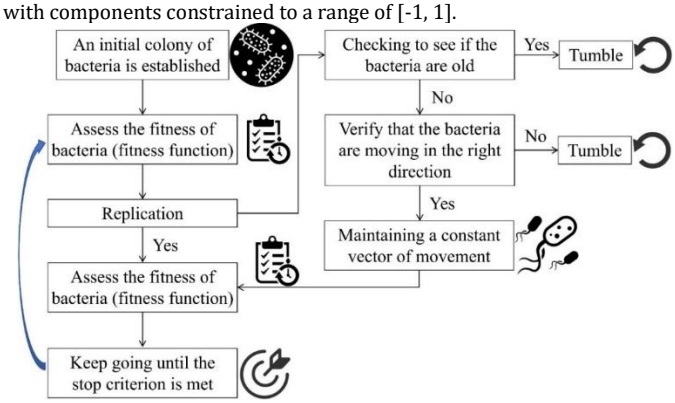

Fig. 3 BFO algorithm

Swarming: As simulated bacteria move, they release attractants and repellants that create cell-to-cell communication. Resulting in complex collective behavior, individuals form swarms that improve exploration efficiency and prevent overcrowding.

Reproduction: An aggregate measure of bacterial fitness or foraging success is used to rank the entire bacterial population. By eliminating the least healthy half of the population, the healthier half can be duplicated, thus preserving and propagating beneficial traits.

Elimination and Diapersal: After several generations of replication, bacteria will undergo elimination-dispersal at a given probability level. Following that, the bacteria will be randomly redistributed to new positions, allowing the global optimal solution to be found.

2.3 Quantification of feature importance

In this study, shapley additive explanation (SHAP) are utilized to identify the salient influencing factors, in order to elucidate the mechanisms underlying the interaction between the failure modes and the punching shear resistance.

This theory calculates and weights the contribution of each feature in all possible feature permutations (Zou et al., 2023). In essence, the objective is to calculate the contribution of each feature to the model output, and to construct an interpretable model that demonstrates properties of superposition from both a global as well as a local perspective. The explanation model can be expressed as follows:

$$f(x) = g(x_s) = \emptyset_0 + \sum_{i=0}^{n} \emptyset_i \cdot x_s^i \quad (7)$$

Where $\emptyset_0$ is a constant value; $\emptyset_i$ denotes the shapley value associated with the i-th feature; n represents the number of input features; x_s^i value determins if the corresponding feature exists, either 0 or 1.

In addition to explaining model performance, SHAP quantifies the predictive influence of features through coalitional permutations. According to the importance of the model output, this metric represents the contribution of each feature to the output and is weighted accordingly (Ma et al., 2023).

3. The dataset and methodology

3.1 Principles and Criteria for Database Establishment

In this study, experimental data for 580 RC slab-column joints have been compiled from published reports (Yan et al., 2025; Shen et al., 2022). An emphasis should be placed on the fact that progressive slab collapse can result in catastrophic structural consequences, whereas the development of a punching cone usually results in abrupt, non-ductile failure of the slab (Shen et al., 2022). In light of this, this study focuses on the mechanisms that govern the evolution of punching cones during failure progression and, as a result, subsumes flexural-punching failure into the broader category of punching shear failure.

The Supplementary data summarizes the preliminary statistical characteristics of each variable, demonstrating that the experimental parameter ranges cover most of the actual parameter ranges and are representative of them. As shown in Fig. 4, each parameter range corresponds to a specific number of samples. Additionally, all subsequent analyses are restricted to studies falling within the parameters described above.

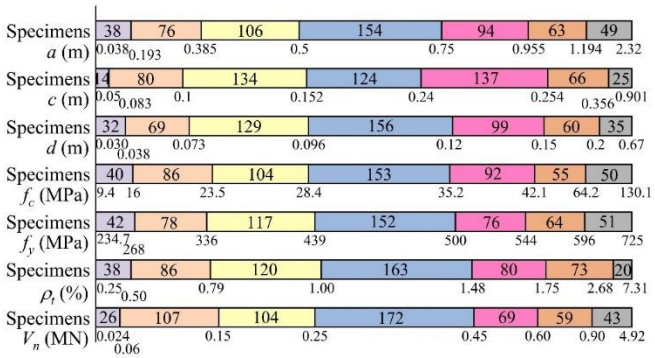

Fig. 4 The parameter interval distribution of experimental specimens

3.2 Definition and scope of input-output variables

In order to investigate the punching capacity of slabs, a detailed description of the inputs and outputs is provided in Table 1. Identifying failure modes and predicting punching shear resistance require distinct analytical approaches. Six input variables are used in failure mode identification: the effective depth of slabs (d); the span to depth ratio (a/d); the column width to critical perimeter ratio (c/b_0); a cube root of the longitudinal reinforcement ratio (ρ_t)$^{1/3}$; the square root of the compressive strength of cylinder concrete (f_c)$^{1/2}$; the strength of flexural reinforcement (f_y). As an output variable, the failure mode classification is expressed in binary notation: 1 for a punching shear failure and 0 for a flexural failure. As an additional input variable, the failure mode is taken into consideration when calculating punching shear resistance.

Table 1. Descriptive summary of the variables

Notation	Unit	Parameters	Type of prediction	
			Failure mode	Resistance
d	m	Effective depth of the slab	Input	Input
a/d	-	Span to effective depth ratio	Input	Input
c/b_0	-	Column width to critical perimeter ratio	Input	Input
$\rho_t{}^{1/3}$	-	A cube root of the longitudinal reinforcement ratio	Input	Input
$f_c{}^{1/2}$	-	The square root of the compressive strength of cylinder concrete	Input	Input
f_y	MPa	The strength of flexural reinforcement	Input	Input
FM	-	Failure mode	Output	Input
V_n	MN	Punching shear resistance	-	Output

Since the dataset contains different units of measurement and numerical ranges, the input feature variables must be normalized. The use of scaling techniques to establish a unified basis for comparison can reduce statistical bias, improving the accuracy of ML models. This can be accomplished by formulating the normalization as follows:

$$x_{i,nor} = \frac{x_i - x_{min}}{x_{max} - x_{min}} \tag{8}$$

Where $x_{i,nor}$ represents the normalized value, x_{min} indicates the minimum value of input values, and x_{max} indicates the maximum value of input values.

3.3 Methodological framework for model development

A total of 580 samples were examined, with 80% (464 cases) being used for training and 20% (116 cases) being used for testing. As the test set has not been trained, it represents unknown data to the model and thus is suitable for the purposes of verifying the model's generalization ability.

In order to develop a ML model for identifying failure modes, the following steps must be followed (Fig. 5): (1) Establishing a dataset using input variables that have been specified; (2) Applying feature scaling to normalize the data; (3) Assembling the dataset into two mutually exclusive subsets, 80% of which were used for training and 20% for testing; (4) Training and testing of the predictive model were performed using three standard ML algorithms (DT, RF, and XGBoost) and two metaheuristic optimization algorithms (GWO and BFO); (5) Making predictions on a reserved test set determines the generalization ability of the selected model.

Table 2. Computational formulas of performance evaluation metrics

Type	Equations	Parameters
Failure modes	$P = \frac{TP}{TP + FP}$ $R = \frac{TP}{TP + FN}$ $Acc = \frac{TP + TN}{TP + FP + TN + FN}$ $F1 = 2 \cdot \frac{P \cdot R}{P + R}$	TP and FP refer to the true positive and false positive predictions at a given decision threshold; TN and FN represent the number of correctly classified negatives and undetected positives.
Punching shear resistance	$\mathrm{MAE} = \frac{1}{m}\sum_{i=1}^{m}\lvert y_{pred,i} - y_{actual,i}\rvert$ $\mathrm{RMSE} = \sqrt{\frac{1}{m}\sum_{i=1}^{m}\left(y_{pred,i} - y_{actual,i}\right)^2}$ $\mathrm{R}^2 = 1 - \frac{\sum_{i=1}^{m}\left(y_{pred,i} - y_{actual,i}\right)^2}{\sum_{i=1}^{m}\left(y_{pred,i} - \frac{1}{m}\sum_{i=1}^{m} y_{actual,i}\right)^2}$	m represents the size of the validation; the predicted and actual values for the ith sample are symbolized as $y_{pred,i}$ and $y_{actual,i}$.

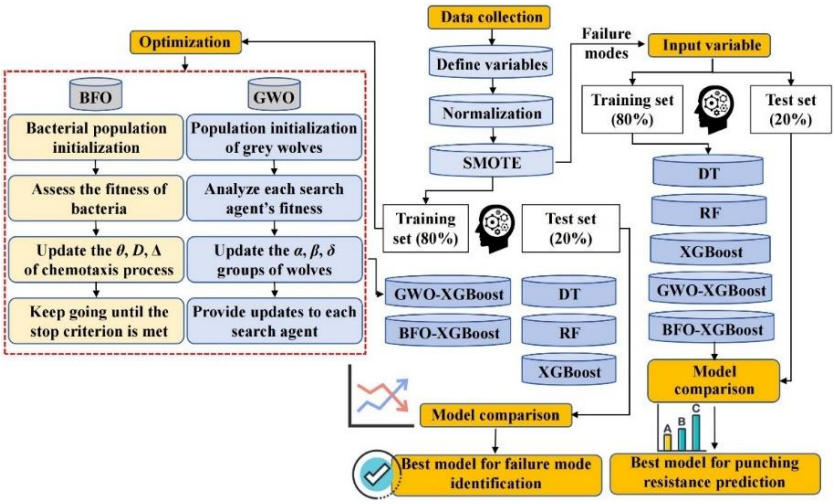

Fig. 5 Flowchart of ML models

The punching shear resistance prediction model is developed by using actual failure as an input variable, and the model can be used to evaluate how different failure modes affect punching resistance.

In failure mode classification, four performance metrics are employed: precision (P), recall (R), accuracy (Acc), F1 score (F1). For punching resistance analysis, three performance metrics are utilized: mean absolute error (MAE), the root mean square error (RMSE), and the coefficient of determination (R^2). Table 2 provides pertinent calculation formulas.

In order to neutralize the underfitting and overfitting biases common to conventional model selection, a combination of fivefold cross-validation (Fig. 6) and swarm-based optimization (Fig. 7) was employed.

Two parameters are critical to optimization behavior of swarm-based algorithms: the number of swarms and the number of iterations. The underfitting of a model can be induced by low values of either parameter. To determine which model would be most effective, we developed BFO-XGBoost and GWO-XGBoost models using four fixed swarm sizes. Table 3 summarizes the optimal parameters for the models under consideration and illustrates the convergence curves in Fig. 7.

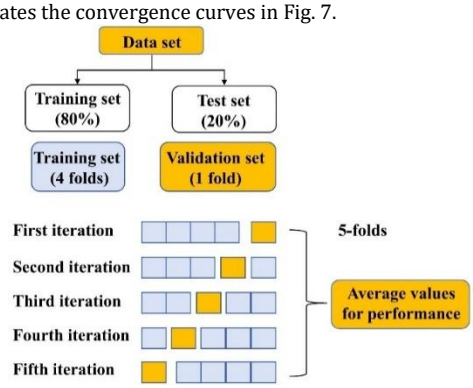

Fig. 6 Fivefold cross-validation

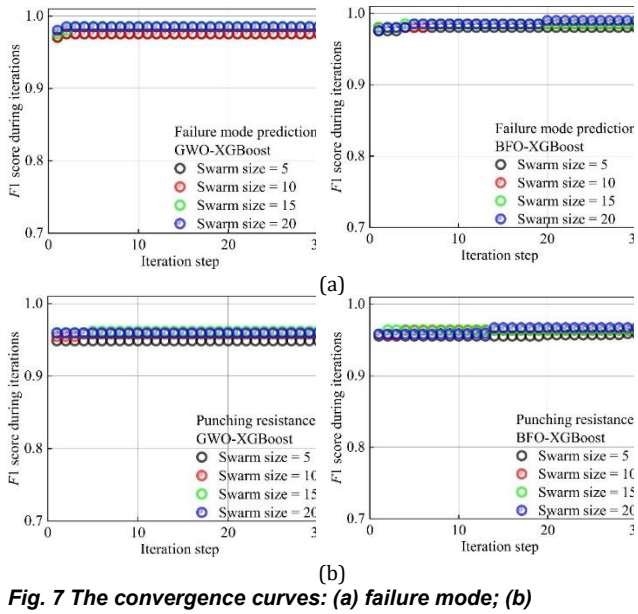

Fig. 7 The convergence curves: (a) failure mode; (b) punching resistance

Table 3. Fundamental hyperparameters of the models

Type of prediction	Algorithms	Parameters
Failure modes	DT	n_estimators=20; max_depth=3
	RF	n_estimators=20; max_depth=3
	XGBoost	n_estimators=20; learning_rate=0.1; max_depth=3
	GWO-XGBoost	learning_rate=0.8538<class'float'>; n_estimators=82<class'int'>; max_depth=4<class'int'>; F1=0.9852.
	BFO-XGBoost	learning_rate=0.4953<class'float'>; n_estimators=43<class'int'>; max_depth=3<class'int'>; F1=0.9900.
Punching shear resistance	DT	min_samples_split=2; max_depth=3; random_state=1
	RF	n_estimators=30; max_depth=3; random_state=1; n_jobs=-1
	XGBoost	random_state=1; n_estimators=30; learning_rate=0.1; max_depth=3
	GWO-XGBoost	learning_rate=0.2388<class'float'>; n_estimators=104<class'int'>; max_depth=5<class'int'>; F1=0.9620.
	BFO-XGBoost	learning_rate=0.1460<class'float'>; n_estimators=200<class'int'>; max_depth=5<class'int'>; F1=0.9672.

Based on Fig. 7(a), GWO-XGBoost achieved optimal performance with a swarm size of 20, corresponding to an F1 score of 0.9852, while BFO-XGBoost achieved optimal performance with an F1 score of 0.9900. According to Fig. 7(b), the GWO-XGBoost model had a F1 score of 0.9622 for a swarm size of 15, whereas the BFO-XGBoost model had a score of 0.9672 for a swarm size of 20.

During failure mode investigation, the Synthetic Minority Oversampling Technique (SMOTE) was employed exclusively on the minority constituents of the training set in order to ensure that class imbalance remediation did not adversely affect the impartiality of the evaluation. In order to avoid bias in the assessment of predictive generalizability, the testing cohort remained unchanged. Comparatively to traditional oversampling methods, SMOTE creates synthetic minorities through interpolation between closely related minorities. In general, the linear interpolation is as follows:

$$p_{i,new} = p_i + \lambda \cdot (p_{i,z} - p_i) \quad (9)$$

Where λ indicates that the interpolation coefficient has been sampled from a uniform distribution spanning the range of 0 to 1; while $p_{i,z}$ corresponds to a random point selected from the set of k nearest neighbors.

4. Results and discussion

4.1 Identification of Failure Modes

According to Table 4, the metaheuristic-optimized GWO-XGBoost and BFO-XGBoost performed significantly better than other ML models. It was found that both hybrid models performed near-perfectly for predicting flexural failures and punching failures on the training dataset, demonstrating the model's ability to predict complex structural failures. Based on the independent test set, the BFO-XGBoost model was found to have the highest accuracy and F1-score, exceeding 98.3% and 93.8%, respectively.

In order to demonstrate the superior performance of the ML approach, the present study includes three empirical models for failure mode classification, whose equations are provided in Table 5. Table 6 summarizes a comparison of the prediction results between the ML models and the empirical equations. There is no doubt that the ML models, particularly the hybrid optimized models, produce significantly higher levels of predictive accuracy than the empirical equations. All performance metrics for the ML models were derived from rigorous independent tests, thus ensuring an unbiased assessment of their generalization performance and representativeness.

Table 4. Comparison of models for determining the mode of failure

Algorithms	Training set				Test set			
	P	R	F1	Acc	P	R	F1	Acc
DT	90.9%	48.1%	62.9%	87.3%	75.0%	40.0%	52.2%	81.0%
RF	87.3%	48.5%	62.3%	87.5%	56.3%	47.4%	51.4%	85.3%
XGBoost	94.5%	54.2%	68.9%	89.9%	73.7%	60.9%	66.7%	88.2%
GWO-XGBoost	100%	100%	100%	100%	68.8%	91.7%	78.6%	94.8%
BFO-XGBoost	100%	98.2%	99.1%	99.8%	93.8%	93.8%	93.8%	98.3%

Table 5. The current empirical models of failure modes

Sources	Equations	Model explanations
Ramdane (1996)	$\phi_1 = \frac{P_{test}}{P_{flex}} = \begin{cases} \leq 1, \text{ punching shear failure;} \\ > 1, \quad \text{flexural failure;} \end{cases}$	fc is the compressive strength of the concrete; u represents the perimeter of critical section; c is the width of the column; B is the perimeter of the slabs
Gesund and Kaushik (1970)	$\phi_2 = \frac{\rho^2 \cdot f_y \cdot d^2}{\sqrt{f_c} \cdot b \cdot u}(10)^4 = \begin{cases} \leq 2, \text{ punching shear failure;} \\ > 2, \quad \text{flexural failure;} \end{cases}$	
Xiao and Chin (2007)	$\phi_3 = \frac{A_s^2 \cdot f_y \cdot d}{80 \cdot c \cdot u \cdot f_t^{1.25}}(\frac{P_{flex}}{P_{punch}}) = \begin{cases} \geq 115, \text{ punching shear failure;} \\ < 115, \quad \text{flexural failure;} \end{cases}$	

Table 6. Comparative analysis with empirical equations

Models	P	R	F1	Acc
Ramdane (1996)	29.2%	9.9%	14.7%	86.0%
Gesund and Kaushik (1970)	40.1%	84.3%	53.3%	83.8%
Xiao and Chin (2007)	34.7%	32.3%	36.9%	84.1%
DT	75.0%	40.0%	52.2%	81.0%
RF	56.3%	47.4%	51.4%	85.3%
XGBoost	73.7%	60.9%	66.7%	88.2%
GWO-XGBoost	68.8%	91.7%	78.6%	94.8%
BFO-XGBoost	93.8%	93.8%	93.8%	98.3%

4.2 Evaluation of punching shear resistance

As shown in Fig. 8, the binary confusion matrix provides a visual representation of the ML model's classification performance. In accordance with the matrix's main diagonal, the entries indicating flexural and punching shear failures are correctly identified. Alternatively, nondiagonal elements represent misclassifications, thereby identifying particular error patterns.

In Fig. 9, the proposed ML models are visually compared with current design standards (ACI 318-2019 and Eurocode 2-2004), while the associated numerical results are summarized in Table 8.

The predictive accuracy of ML models enhanced by hybrid optimization algorithms was evaluated by comparison with collected datasets. As shown in Table 7, the BFO-XGBoost model predicted punching shear resistance with R^2=0.967, MAE= 0.032 MN, and RMSE=0.049 MN during the test phase. Between the predicted and actual values, there is a high degree of alignment. Compared to other ensemble algorithms, BFO-XGBoost and GWO-XGBoost showed superior predictive capabilities. Using this methodology, hyperparameter configurations for the ML algorithm can be tailored to achieve robust, near-optimal results. It appears that hybrid optimization algorithms have effectively mapped the functional relationship between input variables and slab punching shear resistance.

As can be seen from the graph, ML predictions and actual observations are highly correlated. In particular, the BFO-XGBoost model displays a better alignment with the reference line than its counterparts, which is evident from the tighter clustering of data points around the ideal prediction line. Furthermore, the results indicate that the formulations of the design codes are oversimplified, and, as a result, additional critical factors need to be considered. The omission of these variables has been found to significantly reduce the accuracy of model predictions (El-aal et al., 2025; Khajavi et al., 2025). By contrast, the BFO-XGBoost model performs better, with its average ratio ($V_{n,actual}/V_n$) close to unity and covariance near zero. In order to determine the performance of the ML models, a rigorous independent test dataset was used to ensure an unbiased assessment of the generalization ability of the models.

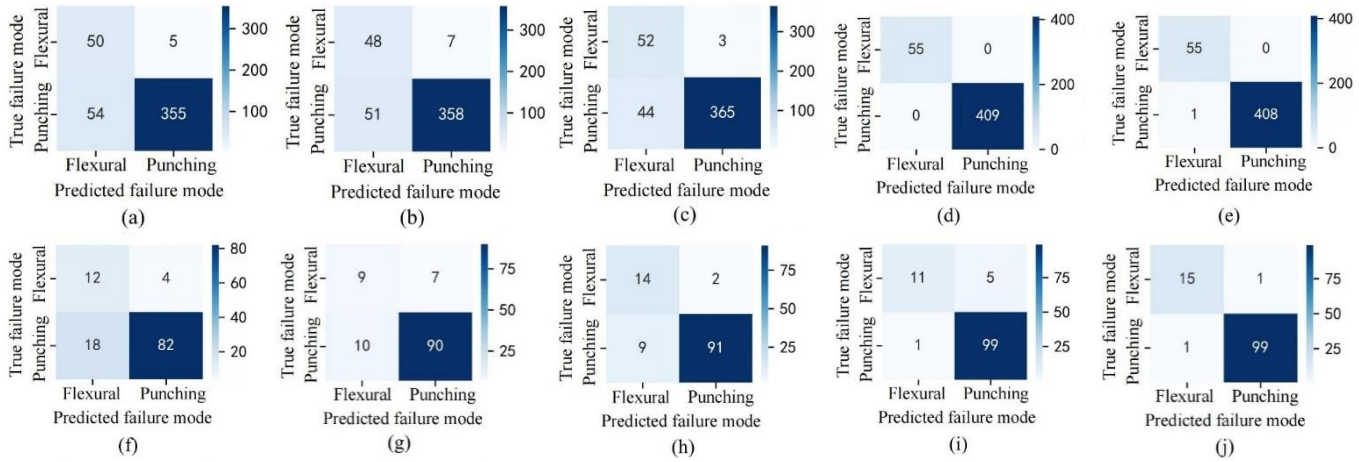

Fig. 8 Matrix of binary confusion for model performance: (a) DT-training; (b) RF-training; (c) XGBoost-training; (d) GWO-XGBoost training; (e) BFO-XGBoost training; (f) DT-test; (g) RF-test; (h) XGBoost-test; (i) GWO-XGBoost test; (j) BFO-XGBoost test.

Table 7. Comparative analysis with empirical equations

ML algorithms	Training set			Test set		
	R^2	MAE(MN)	RMSE(MN)	R^2	MAE(MN)	RMSE(MN)
DT	0.89	0.10	0.14	0.71	0.11	0.15
RF	0.91	0.089	0.13	0.75	0.096	0.14
XGBoost	0.94	0.068	0.11	0.87	0.072	0.099
GWO-XGBoost	0.9993	0.0081	0.011	0.960	0.035	0.053
BFO-XGBoost	0.9996	0.0065	0.0090	0.967	0.032	0.049

Table 8. Summary of punching shear resistance predictions

Method	Avg. ($V_{n,acutal}/V_n$)	Cov. ($V_{n,acutal}/V_n$)	R^2	MAE (MN)	RMSE (MN)
ACI 318-19	1.38	0.31	0.85	0.11	0.16
Eurocode 2-2004	1.20	0.28	0.94	0.62	0.095
DT	0.99	0.45	0.71	0.11	0.15
RF	0.96	0.37	0.75	0.096	0.14
XGBoost	0.98	0.27	0.87	0.072	0.099
GWO-XGBoost	1.0007	0.078	0.960	0.035	0.053
BFO-XGBoost	0.9995	0.072	0.967	0.032	0.049

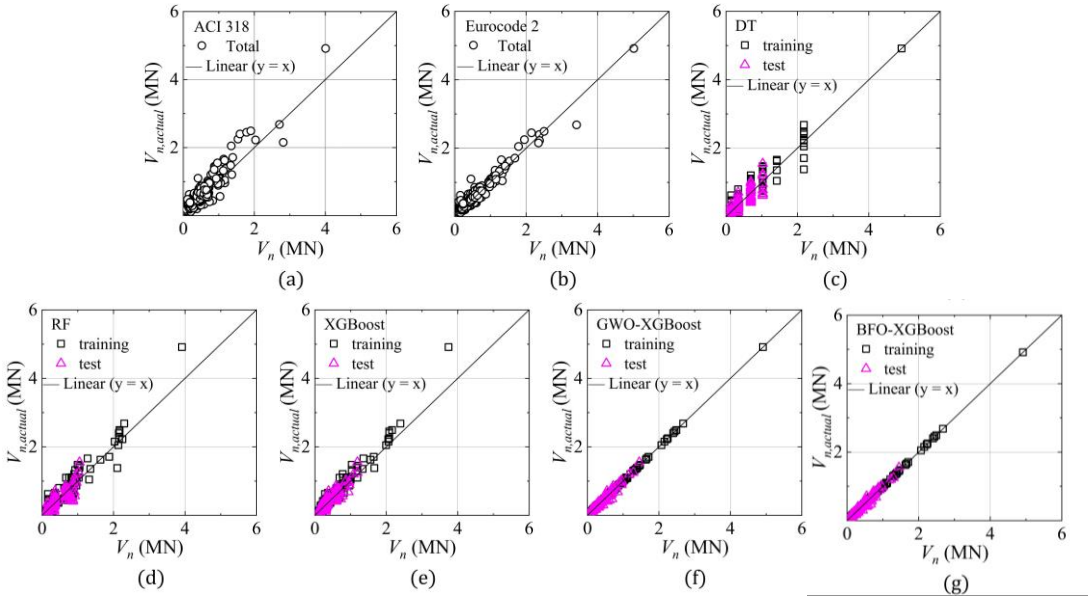

Fig. 9 Comparative analysis of punching shear resistance.

4.3 Interpretive analysis of predictive model behavior

This study utilizes the SHAP method to clarify the decision-making mechanisms of the BFO-XGBoost model, which has demonstrated superior predictive accuracy in previous studies.

Fig. 10(a) illustrates the significance of each input variable in predicting the outcome of the model. Among the factors investigated, $\rho_t{}^{1/3}$ emerges as the most influential, with a SHAP value of 2.97, followed by (f_y, c/b_0, d, $f_c{}^{1/2}$, and a/d). Compared to previous research (Çiftçioglu, 2025; Shen et al., 2022) that has focused primarily on other variables, this study emphasizes the importance of geometric parameter (c/b_0) in failure mode.

In Fig. 10(b), the distribution of feature contributions can be seen, where the color gradient from blue to red indicates the level of influence, ranging from minimal to substantial. According to the prediction, higher values of these parameters ($\rho_t{}^{1/3}$, f_y, and d) indicate an increased probability of punching shear failure. In contrast, the input parameters ($f_c{}^{1/2}$ and a/d) exhibit negative correlations with the outcomes, indicating that higher values are associated with flexural failures, whereas c/b_0 is more complex and requires further analysis.

Fig. 11 shows the plots of feature dependency for failure modes. A threshold-dependent behavior is observed in the probability of punching failure; when $\rho_t{}^{1/3}$ exceeds 1%, the probability increases, while when $\rho_t{}^{1/3}$ is below this critical value, the probability decreases. Similarly, it is found that flexural failure probability increases under three specific points: f_y below 400 MPa, d less than 180 mm, and $f_c{}^{1/2}$ greater than 6.4 ($f_c > 40.9$ MPa). The probability of flexural failure decreases accordingly outside of these parameter ranges. As a result of the parameters c/b_0 (0.11-0.16) and a/d (2.3-6), a greater tendency towards punching shear failure is observed. Alternatively, values outside this range may indicate a greater risk of flexural failure.

The figure provides specific thresholds that can be used to distinguish between two failure mechanisms. It is defined that: when the $\rho_t{}^{1/3}$ exceeds 1%, the f_y is greater than 400 MPa, and the c/b_0 ratio falls within the range of 0.11 to 0.16, the slab-column joints are more likely to experience punching shear failure. The delineation of failure modes provides a practical basis for preliminary failure mode assessment during the design process.

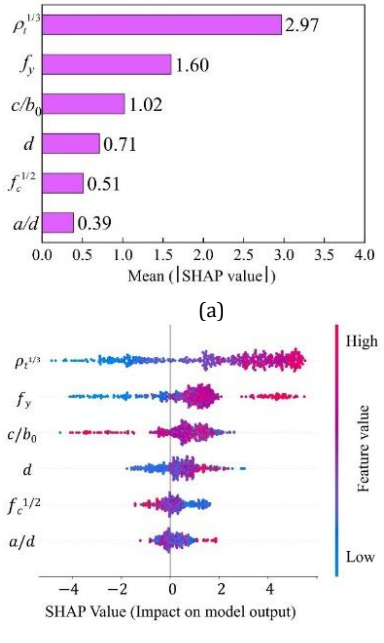

Fig. 10 Global interpretations for failure modes: (a) Statistical significance of each variable; (b) The distribution of feature contributions.

A further investigation of the relationship between the input variables should be conducted beyond the established failure mode discriminators. The $f_c^{1/2}$ and $\rho_t^{1/3}$ are positively correlated, as shown in Fig. 11(e). It can be explained by the fact that an increase in $f_c^{1/2}$ enhances the tensile strength of concrete as well as the bond strength at the interface between concrete and steel. In turn, this synergistic effect creates a more conducive environment for the slab's resistance to be mobilized to its full punching shear capacity.

Fig. 12 illustrates global interpretations of punching shear resistance. A detailed analysis of the SHAP value presented in Fig. 12 (a) reveals the key parameters affecting punching shear resistance. Recent studies have confirmed the fact that d, ρ_t, f_c, f_y, and a/d are the most important factors that determine punching shear resistance (Momani et al., 2024; Alavi et al., 2024; Mellios et al., 2023). In addition, the c/b_0 also appears to be a significant factor in determining both the ultimate resistance and failure mechanism. As compared to other variables, FM has a relatively low impact on ultimate resistance, with a mean SHAP value of 1.9.

It can be seen from Fig.12(b) that the values of d, $\rho_t^{1/3}$, $f_c^{1/2}$, c/b_0 and f_y are positively correlated with the predicted outcomes, indicating that the higher the values of these parameters, the greater the punching shear resistance. In contrast, a decrease in punching resistance can be observed when the a/d ratio increases.

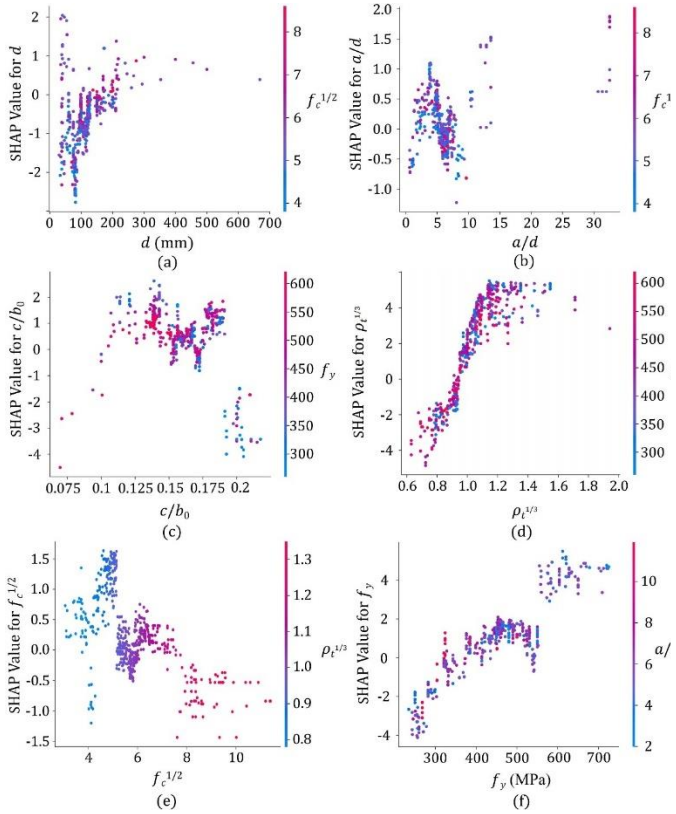

Fig. 11 Plots of feature dependency for failure modes: (a) d; (b) a/d; (c) c/b_0; (d) $\rho_t^{1/3}$; (e) $f_c^{1/2}$; (f) f_y.

Plots of feature dependency for punching shear resistance is shown in Fig. 13. In the case that d exceeds 150 mm, as shown in Fig. 13 (a), further increasing the slab effective depth may increase punching resistance. Due to this, current design codes tend to provide non-conservative estimates of slab effective depths over 200 mm.

In addition, both $\rho_t^{1/3}$ and f_y have a positive effect on the punching shear resistance, especially as $\rho_t^{1/3}$ and f_y rise above 1% and 400 MPa respectively (Fig. 13d and f). In line with previous research findings, these parameters serve as important factors in enhancing the flexural capacity of slabs (Muttoni, 2008; Pang et al., 2021).

Fig. 13(e) shows that $f_c^{1/2}$ values exceeding 6.4 are significantly related to SHAP values, indicating improved punching shear resistance. Considering the observed dual mechanical advantages-enhanced ultimate resistance and reduced sensitivity to brittle punching failure-this study suggests that increasing concrete strength is an effective method for improving the slab-column joint. Fig. 13. Plots of feature dependency for punching shear resistance: (a) d; (b) a/d; (c) c/b_0; (d) $\rho_t^{1/3}$; (e) $f_c^{1/2}$; (f) f_y; (g) FM.

Two geometric parameters (a/d and c/b_0) have the following effects: When a/d is less than 6 and c/b_0 is greater than 0.16, their values have a positive correlation with the SHAP value of the outcomes, and their values increase the punching shear resistance of slab column joints (Figs. 13b and c). In view of the fact that c/b_0 greater than 0.16 is also effective in reducing brittle punching shear failure, this paper recommends that increasing the value of c/b_0 should be given priority to improve punching shear resistance.

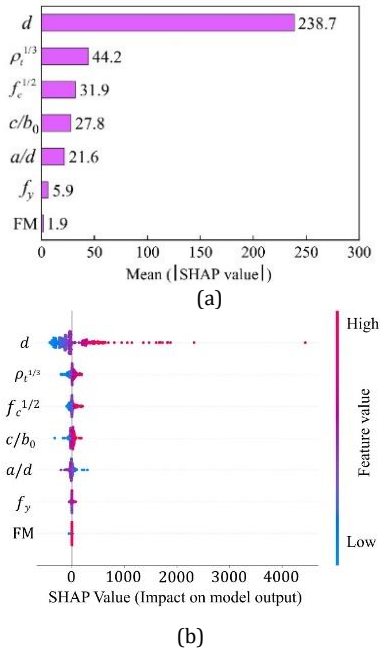

Fig. 12 Global interpretations for punching shear resistance: (a) Statistical significance of each variable; (b) The distribution of feature contributions.

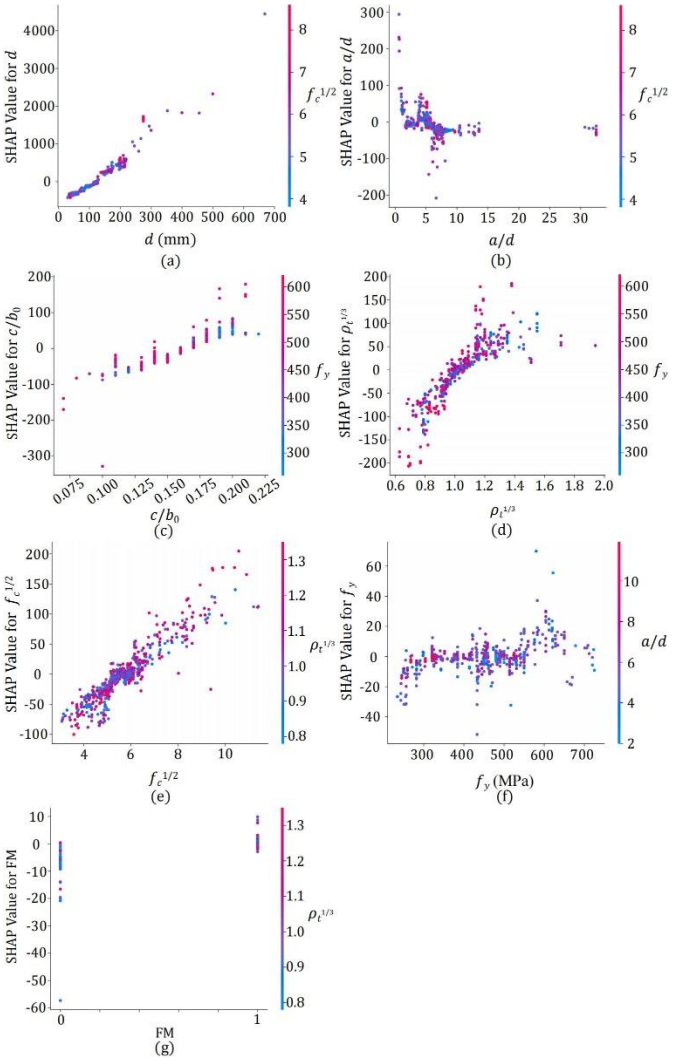

Fig. 13. Plots of feature dependency for punching shear resistance: (a) d; (b) a/d; (c) c/b_0; (d) $\rho_t^{1/3}$; (e) $f_c^{1/2}$; (f) f_y; (g) FM

For this study, parametric correlation analysis is used to quantify the relative magnitude of input variables on both the failure mode and the punching shear resistance. Furthermore, parametric influence analysis is used to identify the range of input variables that have significant effects on specific outcomes. Based on these insights, the paper presents a series

of dual-purpose recommendations that promote punching shear resistance while also promoting more favorable failure modes.

5. Conclusions

In this study, ML models are enhanced with metaheuristic optimization (GWO and BFO) techniques to investigate the relationship between failure modes and the ultimate punching resistance of slab column joints. An in-depth parametric correlation analysis is then performed to determine the model's predictions. In this paper, several interesting results were obtained:

(1) The BFO-XGBoost model performs significantly better than empirical equations and ensemble ML algorithms when it comes to the classification of flexural and punching shear failures.

(2) According to test data, BFO-XGBoost produced perfect punching resistance predictions with R^2 = 0.967, MAE = 0.032MN, and RMSE = 0.049MN, demonstrating the superiority of ML models in solving ultimate resistance problems.

(3) It has been discovered that c/b_0 has a substantial effect on both failure mode and ultimate resistance, which had previously been overlooked. A simplified method for distinguishing between flexural and punching shear failures can be found by comparing $\rho_t{}^{1/3}, f_y$, and c/b_0.

(4) Increasing $f_c{}^{1/2}$ and c/b_0 further can significantly improve ultimate resistance and reduce the risk of brittle punching failures when these values exceed 6.4 and 0.16, respectively.

A limitation of the present ML models is their accuracy in predicting failure modes and ultimate resistance, which are limited by the parameter space from which they were constructed. It is not possible to guarantee predictive confidence for input configurations that lie outside the statistical scope of the dataset used in this study. In light of this, future research efforts should aim to enhance model generalization and prognostic precision through the use of precise numerical analysis and additional experimental datasets.

Acknowledgment

This study was supported by the Shenzhen Science and Technology Program (Grant number: CJGJZD20230724093302005).

Data availability

All data analysed during this study are included in this published article and its supplementary information file.

References

Abbas, Y. M., & Alsaif, A. (2025). Hybrid machine learning models and simplified design formulations for predicting punching shear strength in internal SFRC slab-column connections. Construction and Building Materials 478, 141383. https://doi.org/10.1016/j.conbuildmat.2025.141383

ACI 318-19. (2019). Building Code Requirements for Structure Concrete and Commentary. ACI (American Concrete Institute), Farmington Hills.

Alavi, S. A., Noel, M., Moradi, F., & Layssi, H. (2024). Development of a machine learning model for on-site evaluation of concrete compressive strength by SonReb. Journal of Building Engineering 82, 108328. https://doi.org/10.1016/j.jobe.2023.108328

Alizamir, M., Kim, S., Ikram, R.M.A., Ahmed, K.O., Heddam, S., & Gholampour, A. (2025). A reliable hybrid extreme learning machine-metaheuristic framework for enhanced strength prediction of 3D-printed fiber-reinforced concrete. Results in Engineering 27, 105715. https://doi.org/10.1016/j.rineng.2025.105715

Alkhonaini, M. A., Aljaffan, N., Said, Y., Alsamri, J., Nemri, N., Obayya, M., Alzubaidi, A. A., Alsariera, Y. A., & Alnfiai, M. M. (2025). Leveraging osprey optimization algorithm with deep ensemble learning for cybersecurity in CPS environment. Ain Shams Engineering Journal 16(10), 103612. https://doi.org/10.1016/j.asej.2025.103612

Babiker, A., Abbas, Y. M., Khan, M. I., & Masmoudi, R. (2025). Enhancing design and behavioral understanding of steel fiber-reinforced concrete flat slabs through a robust machine learning framework. Journal of Building Engineering 111, 113133. https://doi.org/10.1016/j.jobe.2025.113133

Çiftçioglu, A. Ö. (2025). Exploring failure mechanisms in reinforced concrete slab-column joints: Machine learning and causal analysis. Engineering Failure Analysis 174, 109549. https://doi.org/10.1016/j.engfailanal.2025.109549

El-aal, S. A., Deifalla, A., Ghali, N. I., & Naim, A. A. (2025). A deep learning model for the punching shear strength of prestressed concrete slabs. International Journal of Machine Learning and Cybernetics 16(10), 7809-7828. https://doi.org/10.1007/s13042-025-02687-w

Erdogan, H. (2024). Strain-Based Grid Beam Model for Predicting Punching Failure of Slab-Column Connections. Arabian Journal for Science and Engineering 49(4), 6007-6026. https://doi.org/10.1007/s13369-023-08420-5

Eurocode 2. (2004). Design of concrete structures – Part 1-1: General rules and rules for buildings. European Committee for Standardization, Brussels.

Ewees, M. H., Gabr, A. S. A., & Farrag, M. R. (2024). Effect of tension and compression flexural reinforcement on punching shear strength of reinforced concrete flat slab. Alexandra Engineering Journal 99, 282-302. https://doi.org/10.1016/j.aej.2024.05.019

Gesund, A., & Kaushik, Y. P. (1970) Analysis of punching shear failures in slabs. In: International Association for Bridge and Structural Engineering, Zurich, Switzerland, pp, 41-60.

Hanoon, D. S., Zareei, S. A., Hassan, R. F., & Zafarani, M. M. (2025). Experimentally investigating hybrid two-way slabs behavior of fiber reinforced concrete slabs casting with different concrete types. Structures 79, 109619. https://doi.org/10.1016/j.istruc.2025.109619

Khajavi, E., Khanghah, A. R. T., & Khiavi, A. J. (2025). An efficient prediction of punching shear strength in reinforced concrete slabs through boosting methods and metaheuristic algorithms. Structures 74, 108519. https://doi.org/10.1016/j.istruc.2025.108519

Kumarawadu, H. R., Weerasinghe, T. G. P. L., & Perera, J. S. (2024). Evaluating the Performance of Ensemble Machine Learning Algorithms Over Traditional Machine Learning Algorithms for Predicting Fire Resistance in FRP Strengthened Concrete Beams. Electronic Journal of Structural Engineering 24(3), 46-52. https://doi.org/10.56748/ejse.24661

Laouissi, A., Benkhelladi, A., Boumaaza, M., Karmi, Y., Hani, M., Belaadi, A., Zaitri, R., Alshaikh, I. M. H., Ghernaout, D., & Chetbani, Y. (2025). Deep neural network modeling of the properties of sustainable high-performance concrete from industrial waste materials. Results in Engineering 27, 106818. https://doi.org/10.1016/j.rineng.2025.106818

Liang, S. X., Shen, Y. X., & Ren, X. D. (2022). Comparative study of influential factors for punching shear resistance/failure of RC slab-column joints using machine-learning models. Structures 45, 1333-1349. https://doi.org/10.1016/j.istruc.2022.09.110

Ma, C. L., Wang, S. X., Zhao, J. P., Xiao, X. F., Xie, C. X., & Feng, X. L. (2023). Prediction of shear strength of RC deep beams based on interpretable machine learning. Construction and Building Materials 387, 131640. https://doi.org/10.1016/j.conbuildmat.2023.131640

Makoond, N., Setiawan, A., Buitrago, M., & Adam, J. M. (2024). Arresting failure propagation in buildings through collapse isolation. Nature 629, 8012. https://doi.org/10.1038/s41586-024-07268-5

Mellios, N., Uz, O., & Spyridis, P. (2023). Data-based modeling of the punching shear capacity of concrete structures. Engineering Structures 275(A), 115195. https://doi.org/10.1016/j.engstruct.2022.115195

Momani, Y., Alawadi, R., Jweihan, Y. S., Tarawneh, A. N., Al-Kheetan, M. J., & Aldiabat, A. (2024). Machine learning-based evaluation of punching shear resistance for steel/ FRP-RC slabs. Ain Shams Engineering Journal 15(5), 102668. https://doi.org/10.1016/j.asej.2024.102668

Monserrat-López, A., Bairán, J. M., de la Fuente, A., & Ruiz, M. F. (2024). Resistance partial factor calibration for SFRC elements without shear reinforcement subjected to punching shear according to EN 1992-1-1:2023. Engineering Structures 343(D), 121219. https://doi.org/10.1016/j.engstruct.2025.121219

Muttoni, A. (2008). Punching shear strength of reinforced concrete slabs without transverse reinforcement. ACI Structural Journal 105(4), 440-450.

Parisi, F., Nettis, A., & Uva, G. (2024). Machine learning-aided cloud analysis for seismic fragility assessment of multi-span bridges. Engineering Structures 343(D), 121175. https://doi.org/10.1016/j.engstruct.2025.121175

Pang, B., Wang, F. L., Yang, J., Nyunn, S., & Azim, I. (2021). Performance of slabs in reinforced concrete structures to resist progressive collapse. Structures 33, 4843-4856. https://doi.org/10.1016/j.istruc.2021.04.092

Ramdane, K. E. (1996). Punching shear of high-performance concrete slabs. In: 4th International Symposium on Utilization of High strength/High-performance concrete, Paris, France, pp, 1015-1026.

Ren, X. D., & Liu, X. P. (2025). Probabilistic modeling and mechanism analysis of punching shear failure of RC slab-column joints based on NGBoost model. Engineering Failure Analysis 182(A), 110057. https://doi.org/10.1016/j.engfailanal.2025.110057

Ren, X. K., Wang, K., Han, X, F., & Zhang, J. Y. (2025). Identification and Damage Detection in Concrete Structures Based on Genetic Algorithm Combined with Cluster Analysis. Electronic Journal of Structural Engineering 25(3), 30-36. https://doi.org/10.56748/ejse.24765

Wang, Z. B. (2025). Hybrid and Ensemble Machine Learning Approaches for Predicting Axial Load Capacity in Rectangular CFST Stub Columns. Electronic Journal of Structural Engineering 25(3), 37-44. https://doi.org/10.56748/ejse.24833

Wu, Y. Q., & Zhou, Y. S. (2022). Prediction and feature analysis of punching shear strength of two-way reinforced concrete slabs using optimized machine learning algorithm and Shapley additive explanations. Mechanics of Advanced Materials and Structures 30(15), 3086-3096. https://doi.org/10.1080/15376494.2022.2068209

Shen, Y. X., Wu, L. F., & Liang, S. X. (2022). Explainable machine learning-based model for failure mode identification of RC flat slabs without transverse reinforcement. Engineering Failure Analysis 141, 106647. https://doi.org/10.1016/j.engfailanal.2022.106647

Tusher, T. H., Ahmed, K. S., Pal, A., Shahjalal, M., & Yazdani, N. (2022). ML models for predicting compressive strength of concrete containing various fibers types. Computers and Concrete 35(6), 645-667. https://doi.org/10.12989/cac.2025.35.6.645

Xiao, R. Y., & Chin, C. S. (2007). Flat slabs at slab-column connection: Nonlinear finite element modelling and punching shear capacity design criterion. Advances in Structural Engineering 10(5), 567-579.

Yan, H. J., & Xie, N. (2024). Optimized Machine Learning Algorithms for Predicting the Punching Shear Resistance of Flat Slabs with Transverse Reinforcement. International Journal of Concrete Structures and Materials, 18(1), 76. https://doi.org/10.1186/s40069-024-00721-9

Yan, H. J., Xie, N., & Shen, D. D. (2025). Hybrid optimized algorithms for predicting punching shear strength in flat slabs considering failure modes. KSCE Journal of Civil Engineering 29(5), 100079. https://doi.org/10.1007/s13369-023-08420-5

Yang, Y., Chen, Y., Zhang P., & Zhang W. N. (2025). Predictive Modeling of Compressive Strength and Slump in High-Performance Concrete Utilizing Machine Learning. Electronic Journal of Structural Engineering, 25(2), 9-16. https://doi.org/10.56748/ejse.25713

Zheng, C. Y., Liu, Y., Liao, Y., Yu, W. H., & Xiong, F. (2025). Flexural behavior of bolted precast concrete floors at the serviceability limit state. Journal of Building Engineering 111, 113215. https://doi.org/10.1016/j.jobe.2025.113215

Zou, D., Wu, L., Hao, Y., Xu, L., & Chen, J. (2023). Composition-strength relationship study of ultrahigh performance fiber reinforced concrete (UHPFRC) using an interpretable data-driven approach. Construction and Building Materials 392, 131973. https://doi.org/10.1016/j.conbuildmat.2023.131973

Disclaimer